3 The interaction of particles and γ-radiation with matter

The penetration of ionizing radiations into matter has been of theoretical interest and of practical importance for nuclear physics since the early days of the subject. The classification of the radiations from radioactive substances as α-, β- and γ-rays was based on the ease with which their intensity could be reduced by absorbers. Range or absorption coefficient provided, and still provides, a useful method of energy determination, and the associated processes of ionization and excitation underlie the operation of nearly all present-day particle and photon detectors. In the present chapter the basic processes of the interaction of radiation will be examined with particular reference to their role in nuclear techniques.

The interaction of nuclei with matter may also be taken to include hyperfine effects in spectroscopy and perhaps even the formation of exotic atoms in which an ordinary electron is replaced by a heavier particle. These structures give much information both on nuclei and particles and will be briefly reviewed.

3.1 Passage of charged particles and radiation through matter

3.1.1 General

For energies up to a few hundred MeV, the main process by which a charged particle such as a proton, α-particle or meson loses energy in passing through matter is the transfer of kinetic energy to atomic *electrons*, with very little deviation from the original path. The more energetic recoil electrons produced in this way are visible along the track of a charged particle in an expansion chamber as *delta rays*. In special cases, e.g. for fission fragments or other heavy ions, transfer of energy to the nuclei of the medium may also be important. In such cases of high charge, or low velocity or both, *large-angle scattering* by Coulomb interaction with the nuclei may be observed, but for fast, light ions this is a rare event. It is consequently reasonable, at least for such particles, to define a definite *range* in matter (Fig. 3.1a).

Fast electrons and positrons also lose energy by collision with other electrons and may be scattered through angles up to 90° in such collisions. They lose very little energy to nuclei, because of the disparity in mass, but can suffer large deflections, >90°. In all collisions in which accelerations are experienced, electrons and positrons also lose energy by the radiative process known as *bremsstrahlung.* Heavy particles do not radiate appreciably in this way
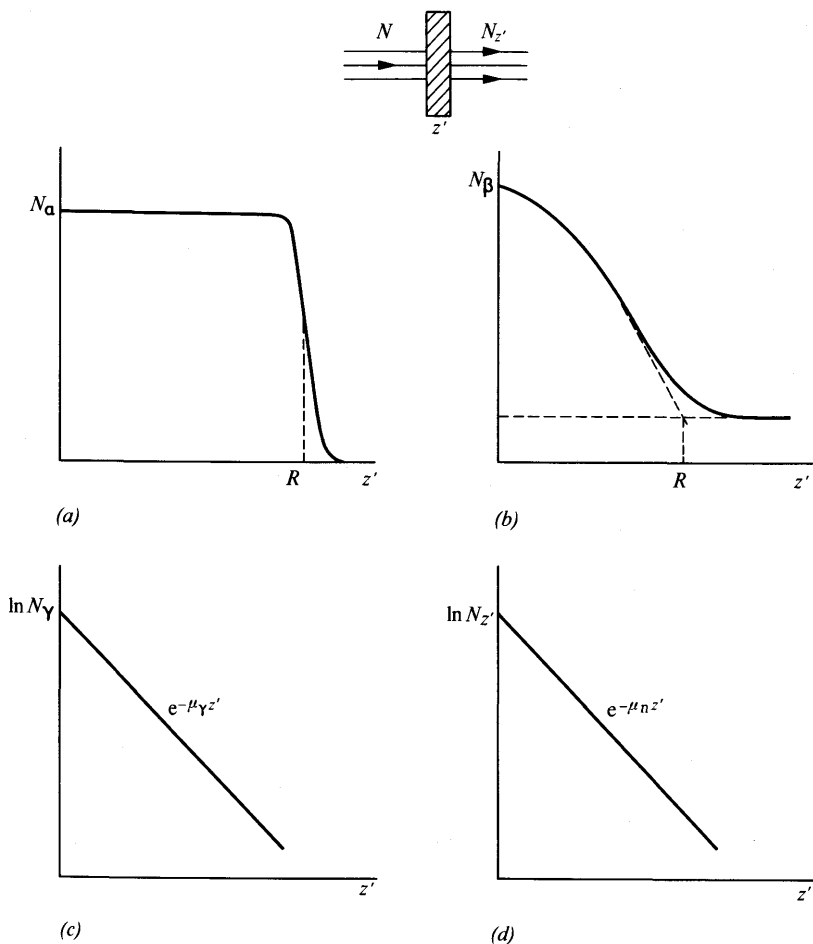

Fig. 3.1   Absorption of initially homogeneous particles by matter (schematic): (*a*) Light ions (e.g. α, p, muons) showing mean range *R*. (*b*) Electrons, showing extrapolated range *R*. (*c*) Photons, $E_\gamma < 10$ MeV. (*d*) Neutrons. Absorber thicknesses z' and ranges *R* are conveniently measured as mass per unit area of absorber (ρ_s), and μ in (*c*) and (*d*) is then a mass absorption coefficient.

because their accelerations are much smaller. As a result of scattering and radiative energy loss, a group of initially monoenergetic electrons may traverse considerably different thicknesses of matter before being brought to rest, and range can best be defined by an extrapolation process (Fig. 3.1*b*).

Electromagnetic radiation interacts with matter through the processes of elastic (Rayleigh and nuclear) scattering, photoelectric effect, Compton effect and pair production. These processes reduce the *number* of photons in a beam in proportion to the number incident on an absorber; thereby creating an exponential attenuation (Fig. 3.1*c*). No definition of range is appropriate, although the attenuation coefficient is energy-dependent. For radiation of energy above say 10 MeV, the electrons and positrons from the pair-production process themselves generate bremsstrahlung and annihilation quanta and an electromagnetic shower builds up characterized by a linear dimension called the *radiation length* (Sects. 2.1.5 and 3.1.3).

At energies above about 100 MeV the *nuclear interactions* of charged particles, other than leptons, are no longer negligible compared with electronic and nuclear collision losses. These interactions remove particles from a beam and the low-energy concept of range must be replaced in effect by an attenuation coefficient based on total nuclear cross-sections (including scattering). An absorption plot resembling Fig. 3.1c then replaces the range curve Fig. 3.1*a*. Such plots are very clearly shown in the case of *neutrons* of all energies for which there is only nuclear attenuation (Fig. 3.1*d*).

The relative importance of collision and radiative energy loss for electrons and protons in lead is shown in Fig. 3.2.
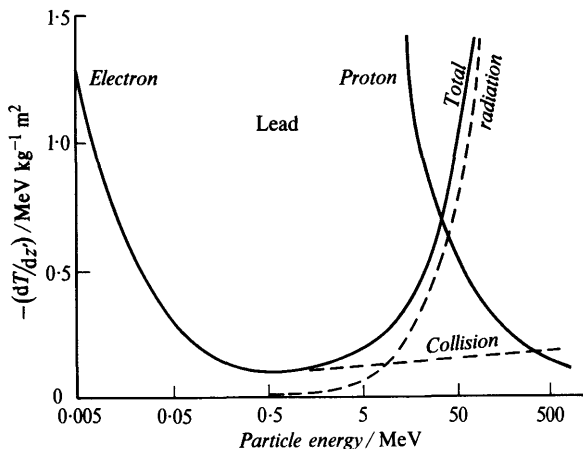

Fig. 3.2   Energy loss for electrons and protons in lead as a function of kinetic energy (Heitler, W., *The Quantum Theory of Radiation*, Clarendon Press, 1954).

3.1.2 Energy loss by collision

If a particle of charge $Z_1 e$ and velocity $v = \beta c$ passes through a substance of atomic weight A (kg) and atomic number Z the energy loss dT in a path dz' (where z' is measured by the surface density ρ_s, in $\mathrm{kg\,m}^{-2}$) is given by the Bethe–Bloch formula

$$-\left(\frac{dT}{dz'}\right)_{\mathrm{coll}} = \frac{1}{(4\pi\varepsilon_0)^2} \frac{2\pi N_A Z Z_1^2 e^4}{m_e v^2 A}$$
$$\times \left[\ln \frac{2m_e v^2 W_{\mathrm{max}}}{I^2(1-\beta^2)} - 2\beta^2 - \delta - U\right] \quad (3.1)$$

where I is a mean excitation potential for the atoms of the substance. If there are no radiative losses, this is the *stopping power* of the absorber for velocity v; it has the unit energy $\times \mathrm{kg}^{-1}\,\mathrm{m}^2$.

W_{max} is the maximum energy transfer from the incident particle to an atomic electron, given by

$$W_{\mathrm{max}} = 2m_e v^2/(1-\beta^2) \text{ for energies} \ll M_1^2 c^2/2m_e \quad (3.2)$$

δ is a correction for polarization of the medium and U allows that inner shell electrons do not necessarily behave as free electrons.

The rigorous derivation of formula (3.1) is a quantum mechanical problem of some complexity and will not be attempted here. The general form of the main term, however, can be indicated classically as follows:

Assume (Fig. 3.3) that the incident particle moves in a straight line at a perpendicular distance b (the impact parameter of Sect. 1.2.6) from a stationary electron. The impulse conveyed to the electron by the passage of the particle is then

$$q = \int F \, dt \approx 1/4\pi\varepsilon_0 \cdot Z_1 e^2/b^2 \cdot 2b/v \quad (3.3)$$

where F is the perpendicular component of the force acting on the electron during passage from A to B, which may crudely be assumed to represent the distance over which a constant force
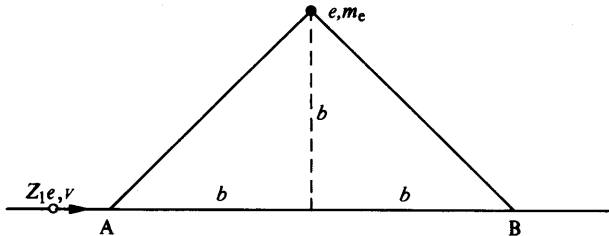

Fig. 3.3 Energy loss of a charged particle to an electron at impact parameter b.

$Z_1 e^2/b^2$ is effective. The energy transferred to the electron is

$$q^2/2m_e = (1/4\pi\varepsilon_0)^2 (2Z_1^2 e^4/m_e v^2 b^2) \qquad (3.4)$$

The number of electrons per unit thickness with impact parameters between b and $b + db$ is $2\pi b\, db \times N_A Z/A$ so that the differential energy loss per unit thickness for this range of b is

$$-d^2T/dz'\, db = (1/4\pi\varepsilon_0)^2 (4\pi N_A Z Z_1^2 e^4/m_e v^2 A b) \qquad (3.5)$$

Integration between limits b_{max} and b_{min}, corresponding to energy losses for which a simple theory is valid, gives

$$-dT/dz' = (1/4\pi\varepsilon_0)^2 (4\pi N_A Z Z_1^2 e^4/m_e v^2 A) \ln (b_{max}/b_{min}) \qquad (3.6)$$

which agrees with the first term of (3.1) using the value of W_{max} given by (3.2) if

$$b_{max}/b_{min} = 2m_e v^2/I(1-\beta^2) \qquad (3.7)$$

Reasons can be given for this ratio of extreme impact parameters (Ref. 3.1). Thus b_{max} is determined by the fact that no energy transfer takes place when the time of collision $\approx 2b/v$ becomes long compared with atomic frequencies so that the collision is adiabatic. Also, b_{min} is related to the validity of the classical treatment of the collision, which will break down when the de Broglie wavelength of the electron in the c.m. system approaches b.

The stopping-power formula, equation (3.1), predicts a variation of dT/dz' with energy similar to the experimental results for protons in aluminium which are shown in Fig. 3.4; it will be noted that m_e is the mass of the *electron* and not the mass M_1 of the incident heavy particle. The simple theory is not strictly valid at low energies, partly because of the neglect of the effect of capture and loss of electrons by the moving particle. The appearance of a maximum in the observed collision loss is at least partly due to this, although it is also predicted by the velocity dependence shown in equation (3.1). At higher energies the energy loss falls off as $1/v^2$ with increasing v to the point of *minimum ionization*, beyond which is seen the *relativistic rise* due to the $(1-\beta^2)$ term, with $\beta \approx 1$ and γ (Fig. 3.4) = $(1-\beta^2)^{-1/2}$.

In placing equation (3.1) on an absolute scale the principal uncertainty is in the atomic excitation potential I. It may be obtained from measurements of stopping power or from calculations based on an atomic model; both indicate that

$$I = kZ \text{ eV}$$

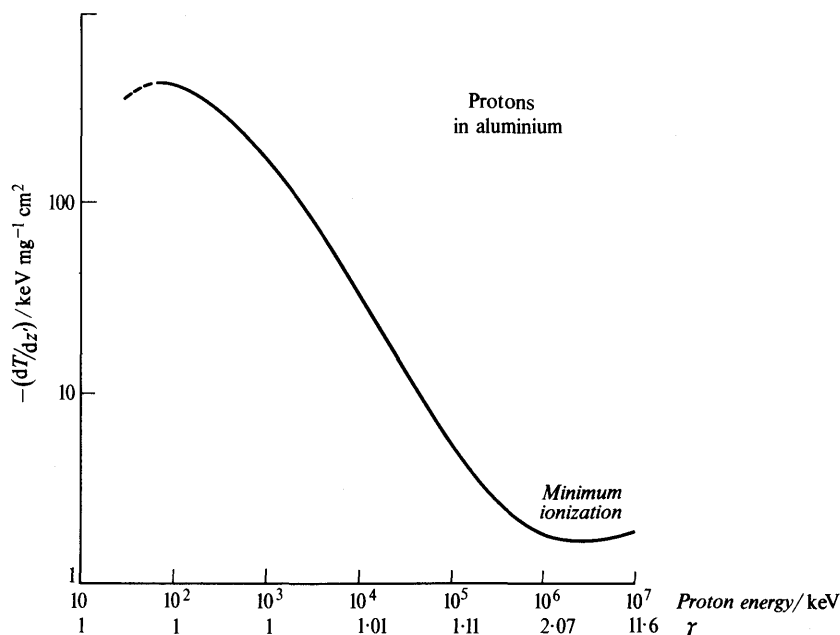where $k \approx 11$, with some dependence on Z for very light and very heavy atoms.

Fig. 3.4 Specific energy loss, or stopping power, of aluminium for protons. The quantity $\gamma = (1 - \beta^2)^{-1/2}$ is the Lorentz factor.

Observable phenomena basically governed by the collision-loss formula for a single particle are:

(a) Production of ion pairs in solids, liquids and gases and of electron-hole pairs in semiconductors.
(b) Production of light in scintillator materials.
(c) Production of bubbles in a superheated liquid.
(d) Production of developable grains in a photographic emulsion.

Each of these has been made the basis of an energy-sensitive particle detector.

3.1.3 Energy loss by radiative processes

Electrons of kinetic energy T and total energy E passing through a thin absorber give rise in each radiative collision to a bremsstrahlung photon of any energy between 0 and T. The process may be envisaged as in Fig. 3.5, in which the Coulomb field existing between the incident electron and a nucleus, or another electron, of the absorbing medium is represented by an emission of virtual photons. The real electron makes a Compton scattering collision

78

(Sect. 2.1.4) with a virtual photon, creating a virtual lepton, which then gives rise to a real photon, i.e. the bremsstrahlung quantum and a real electron of reduced energy. The bremsstrahlung process $e \rightarrow e' + \gamma$ cannot take place in free space because momentum and energy cannot then be conserved. Photons can however also be emitted by electrons moving in the magnetic field of an orbital accelerator (Sect. 4.3.3) and this emission is known as *synchrotron radiation.*

The energy distribution of the bremsstrahlung is given by the expression (Ref. 3.1)

$$\phi(E, \nu) \, \mathrm{d}\nu \propto Z^2 f(E, \nu) \, \mathrm{d}\nu/\nu \qquad (3.8)$$

where for energies $T \approx 100 \, \text{MeV}$ at least $f(E, \nu)$ varies only slowly with the frequency ν. The energy *loss* $h\nu\phi \, \mathrm{d}\nu$ in each frequency interval is then constant to a first approximation. By integrating over the available frequency spectrum the energy loss per unit path in kg m^{-2} at kinetic energy T is

$$-(\mathrm{d}T/\mathrm{d}z')_{\text{rad}} = N_A/A \int_0^{T/h} h\nu\phi(E, \nu) \, \mathrm{d}\nu \qquad (3.9)$$

and because of the slow variation of $h\nu\phi$ with ν the integral is

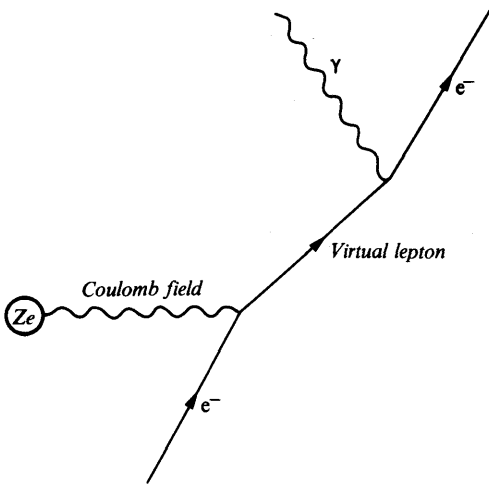Fig. 3.5   Production of bremsstrahlung by an electron in the field of a nucleus Ze; the virtual lepton is an electron 'off the mass shell'. This and subsequent similar figures are not intended to display the precise order of events, and other diagrams showing a different order may be drawn. Time increases to the top of the page, and a fixed Coulomb field is shown as a wavy horizontal line. Rules exist for calculating cross-sections from such graphs.

approximately proportional to the incident (total) energy E, i.e.

$$-(dT/dz')_{rad} = E \cdot N_A/A \cdot \bar{\phi} \qquad (3.10)$$

where $\bar{\phi}$ is a calculable function.

At high energies, collision loss (eqn (3.1)) varies as $\ln(1-\beta^2)^{-1}$ i.e. as $\ln E$, while radiative loss (eqn (3.10)) is proportional to E and therefore predominates. The electron energy at which the two losses are equal is the *critical energy E_c*. When radiative loss is dominant it is useful to define a *radiation length X_0* by the equation

$$-dz'/X_0 = dE/E \qquad (3.11)$$

so that X_0 is the absorber thickness over which the electron energy is reduced by a factor e. Table 3.1 gives critical energies and radiation lengths for a few common materials.

TABLE 3.1   Critical energy and radiation length (from Ref. 3.1)

Material	E_c/MeV	X_0/kg m^{-2}
H	340	580
C	103	425
Fe	24	138
Pb	6·9	58
Air	83	365

Classically, bremsstrahlung originates in the acceleration of a charged particle as a result of Coulomb interaction, and its intensity is therefore inversely proportional to the square of the particle mass according to Maxwell's theory. The muon has 200 times the electron mass and its radiative energy loss is therefore negligible. This holds *a fortiori* for all other charged particles, since they are heavier still.

All charged particles independently of their mass do, however, suffer a small electromagnetic loss in matter through *Cherenkov radiation*. This depends on the gross structure of the medium through which the particle passes, and in which a macroscopic polarization is set up. If the velocity of the particle exceeds the velocity of light in the medium, the polarization is longitudinally asymmetric and secondary wavelets originate along the track AB of the particle (Fig. 3.6). These form a coherent wavefront propagating in a direction at angle θ with the path of the particle where

$$\cos\theta = c/n \div \beta c = 1/\beta n \qquad (3.12)$$

n being the refractive index. The process is analogous to the formation of the bow wave of a ship. It has the important features for nuclear detectors that coherence does not appear until $\beta = 1/n$, i.e. there is a *velocity threshold* for observable radiation, and also that the direction of emission is very well defined.
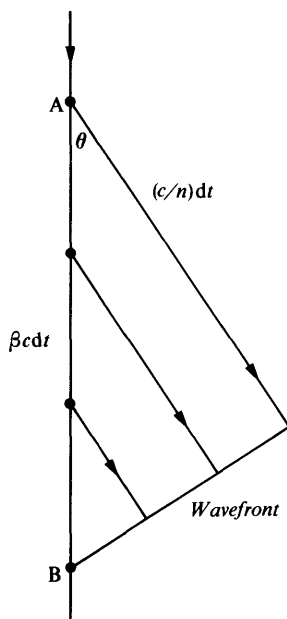
Fig. 3.6   Formation of a coherent wavefront of Cherenkov radiation.

Cherenkov loss is usually only about 0·1 per cent of collision loss. Explicitly, the loss for a singly charged particle may be written

$$-\left(\frac{dT}{dz}\right)_{Ch} = \frac{\pi e^2}{c^2 \varepsilon_0} \int \left(1 - \frac{1}{\beta^2 n^2}\right) \nu \, d\nu \qquad (3.13)$$

where the integration extends over all frequencies for which $\beta n > 1$. Within these bands the spectral distribution of loss is proportional to $\nu \, d\nu$ in contrast with the $d\nu$ proportionality of bremsstrahlung. Cherenkov light is thus found mostly at the blue end of the visible spectrum.

3.1.4 Absorption of electromagnetic radiation

As discussed in Section 1.2.5 the attenuation of a beam of photons by matter is described by equation (1.35a), namely

$$n = n_i \exp\left(-\mu_m \rho_s\right) \qquad (3.14)$$

where μ_m is the mass attenuation coefficient ($m^2 \, kg^{-1}$) and ρ_s is the mass per unit area of the absorber. The same formula describes the diminution of the *intensity* $n_i \times h\nu$, or energy flux.

81

To relate the measured μ_m to calculated cross-sections for interactions with absorber atoms, it may be necessary first to correct for the fact that both elastic (Rayleigh) and inelastic (Compton) scattering give scattered photons of the incident energy in the forward direction, i.e. the direction of the incident beam. The Rayleigh scattering may in many cases be neglected since it is sharply forward-peaked at high energies and does not remove photons from the beam unless collimation is very fine. Compton scattering, on the other hand, does not depend sharply on angle at small angles and may result in some solid-angle dependence of the absorption coefficient. This cannot easily be avoided by energy discrimination because the energy change is small near the forward direction. It may be corrected both experimentally, by making measurements in different geometries, and theoretically.

When such corrections have been made we may write $\mu_m = N_A \sigma / A$ with

$$\sigma = \sigma_{PE} + Z\sigma_C + \sigma_{PP} \qquad (3.15)$$

The individual cross-sections relate to the photoelectric effect, the Compton effect and pair production respectively, and the factor Z embodies the assumption that all the atomic electrons contribute individually (and incoherently) to Compton scattering. This will be true if the photon energy is much greater than the K-shell ionization energy of the atom.

The relative importance of the three absorption processes as a function of energy and of atomic number is shown in Fig. 3.7 and the actual mass absorption coefficient μ_m for lead is given as a function of energy in Fig. 3.8. This curve shows: (a) sharp peaks at
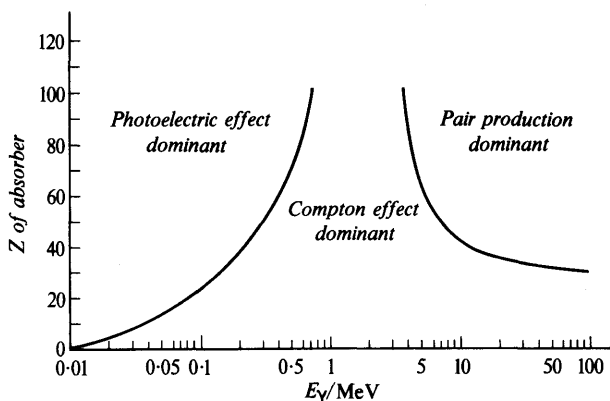

Fig. 3.7   Relative importance of the three major types of γ-ray interaction (Ref. 2.1).
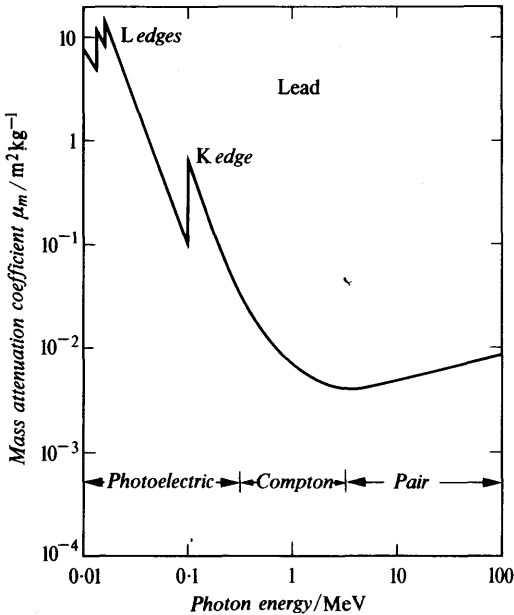
Fig. 3.8   Mass attenuation coefficient for electromagnetic radiation in lead (Ref. 2.1).

energies corresponding with the atomic absorption edges and indicating the onset of increased photoelectric absorption as a new electron shell becomes available; and (*b*) a minimum absorption coefficient due to the compensation of photoelectric and Compton cross-sections that fall with energy by the pair production cross-section that rises. Both effects mean that the energy is not a single-valued function of μ_m throughout its range for a given absorbing material.

The individual processes indicated in equation (3.15), together with elastic scattering, are all part of the total electromagnetic interaction between radiation and matter and are therefore connected. For most practical purposes, in the energy range of interest to nuclear physics, it is possible to regard them as independent, each contributing to the total cross-section to a degree determined by the quantum energy. The salient features of the processes are as follows:

(i) *Photoelectric effect* (Fig. 3.9).   Because of the necessity to conserve energy and momentum, a free electron cannot wholly absorb a photon. Photoelectric absorption, therefore, tends to take place most readily in the most tightly bound electronic shell of the atom available, since then momentum is most easily conveyed to the
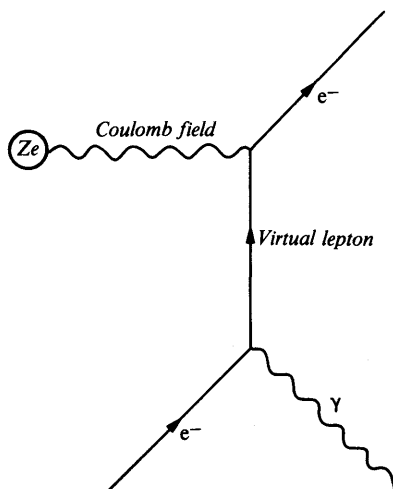
83

Fig. 3.9 Photoelectric effect; conservation of momentum and energy require interaction with the atom, Ze.

atom. The kinetic energy of a photoelectron from the K-shell is

$$T = h\nu - E_K \qquad (3.16)$$

where E_K is the K-ionization energy. The cross-section depends on atomic number Z and wavelength of radiation λ approximately as

$$\sigma_{PE} \approx Z^5 \lambda^{7/2} \qquad (3.17)$$

in the energy range $0 \cdot 1$ to $0 \cdot 35$ MeV. The vacancy in the atom created by the ejection of a photoelectron leads to the emission of characteristic X-rays or of electrons known as *Auger electrons* from less tightly bound shells as an alternative process favoured for light atoms.

(ii) *Compton effect* (Figs. 2.3 and 3.10). The scattering of photons by atomic electrons that may be regarded as free should be treated relativistically. In Section 2.1.4 this collision process was described as evidence for the photon hypothesis, and it was shown that conservation of 4-momentum leads to a relation between the wavelength of the incident photon and that of the scattered photon emerging at an angle θ with the original direction (eqn (2.7)):

$$\lambda' - \lambda = c/\nu' - c/\nu = (h/m_e c)(1 - \cos \theta) \qquad (3.18)$$

where $h/m_e c$ is the Compton wavelength of the electron $(2 \cdot 43 \times 10^{-12}$ m$)$. The energy of the recoil electron is $h(\nu - \nu')$; it is zero for $\theta = 0$ and a maximum for $\theta = \pi$.
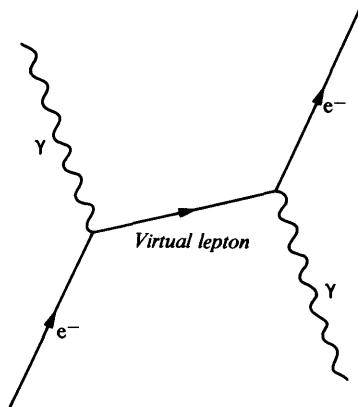
Fig. 3.10   Compton effect, with free electron.

The Compton wavelength shift is independent of wavelength and of the material of the scatterer. The differential cross-section for the process is given by a formula due to Klein and Nishina, which predicts that at a given angle the cross-section decreases with increasing photon energy. The angular variation for a range of energies is shown in Fig. 3.11; in all cases there is a finite cross-section for $\theta = 0$ and equation (3.18) shows that over a small angular range about zero the wavelength is essentially unmodified.

As $h\nu/m_e c^2$ tends to zero the angular distributions shown in Fig. 3.11 become more symmetrical about 90° and finally reach the form $(1 + \cos^2 \theta)$ characteristic of classical *Thomson scattering*. However, the assumption of scattering from free electrons then becomes less tenable for matter in its normal state, and coherent *Rayleigh scattering* from the bound electrons forming the atomic charge distribution takes over.

(iii) *Pair production* (Fig. 3.12).   The process

$$h\nu \rightarrow e^+ + e^- \qquad (3.19)$$

like the bremsstrahlung process (Sect. 3.1.3), cannot take place in free space because 4-momentum conservation cannot be satisfied. If a third electron or, better still, a nucleus is present to absorb recoil momentum, pair production occurs in accordance with the diagram of Fig. 3.12. For pair production in a nuclear field the threshold energy is $2m_e c^2$, i.e. 1·02 MeV.

Following Dirac's theory of holes (Sect. 2.1.5), the process may be pictured as the elevation of an ordinary electron from a *negative energy state* $(E \leqslant -m_e c^2)$ to a normal positive state $(E \geqslant m_e c^2)$, for which an energy consumption of at least $2m_e c^2$ is required. The hole
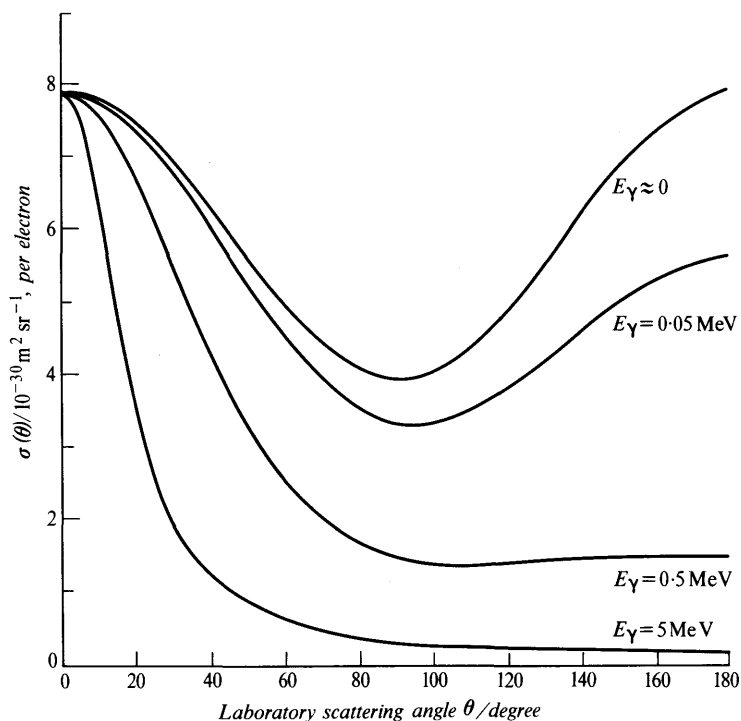
85

Fig. 3.11 Differential cross-section for Compton scattering, giving *number* of photons scattered per unit solid angle at angle θ, for energies 0–5 MeV.
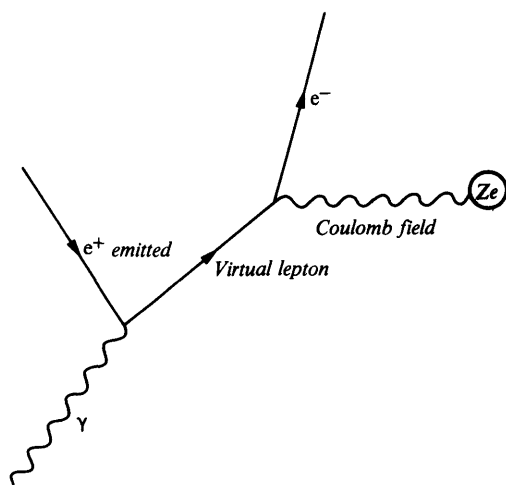

Fig. 3.12 Pair production, in nuclear field. The motion of an electron backwards in time corresponds to the *emission* of a positron.

left in the normally filled band of negative states then behaves as a positive electron. Alternatively, in terms of Fig. 3.12, the antiparticle or positron may simply be regarded as a normal particle moving backwards in time.

The exact converse of process (3.19) is the transition of an ordinary electron to a state of negative energy with the emission of a single quantum of annihilation radiation, rather than the two quanta normally produced. This is just a bremsstrahlung process, as may be seen by comparing Figs. 3.5 and 3.12, and indeed the two processes are both described by the theory due to Bethe and Heitler. In each case the cross-section varies as Z^2, and decreases at first as the primary photon (or electron) energy increases. This corresponds to the production of pairs at larger and larger distances from the nucleus, but a limit is set by the screening of the nuclear charge by the atomic electrons. The variation of σ_{PP} with energy is shown for lead, with and without screening, in Fig. 3.13.
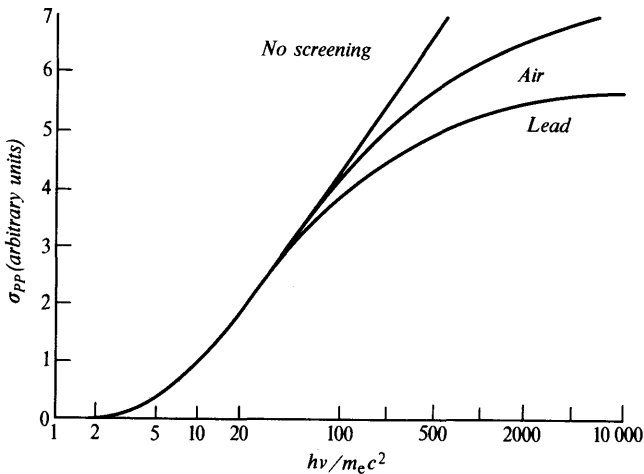

Fig. 3.13   Effect of screening on pair production cross-section for air and lead (Ref. 3.1).

3.2 Experimental studies

The theoretical results outlined in Section 3.1 are applied mainly in the determination of the energy of known particles, including photons, and in identifying unknown particles and finding their mass. In such work several more detailed features of the general energy-loss process and deductions from it must be considered, and these are treated in the following sections.

3.2.1 Multiple Coulomb scattering

In the passage of a charged particle through matter, small-angle deflections are continually arising because of distant Coulomb interactions with nuclei and electrons. These accumulate in a random manner to produce a resultant deviation which has a Gaussian distribution for a group of particles. This distribution of angles may be written

$$P(\theta)\, d\theta = (2\theta/\langle\theta^2\rangle) \exp(-\theta^2/\langle\theta^2\rangle)\, d\theta \qquad (3.20)$$

and according to Rossi and Greisen

$$\langle\theta^2\rangle = (Z_1^2 E_s^2/p^2\beta^2 c^2) z'/X_0 \qquad (3.21)$$

where E_s is a constant (21 MeV) independent of the mass of the particle and the nature of the medium, p is the particle momentum, z' is the path in the medium, assumed large, and X_0 is the radiation length (Sect. 3.1.3).

Multiple scattering limits the precision of momentum and angle measurements on particle tracks. For a proton of momentum 10 GeV/c, observed in a hydrogen bubble chamber in a magnetic field, multiple scattering introduces an uncertainty comparable with errors of measurement. For heavy ions there are noticeable deviations from the simpler theories.

3.2.2 Range–energy curves; straggling

The theoretical range of a heavy charged particle is equal to its path length in matter because over most of the path scattering is negligible. The range may formally be obtained by integration of the expression for energy loss, giving

$$R = \int_0^T dT(dT/dz')^{-1} \qquad (3.22)$$

but in practice this cannot be carried out for the full range of the particle because of the corrections necessary to the explicit formula for dT/dz' at low energies. Range–energy curves are therefore constructed semi-empirically by combining observations of the range of particles of known energy with integrations of the energy-loss formula over some particular region.

The first range–energy curve to be established was for α-particles in air. Energies of α-particles from radioactive elements were obtained from the classical magnetic deflection experiments of Briggs, Rosenblum and Rutherford with a precision of 1 part in 10^5 in favourable cases. Ranges were measured by observing tracks in an expansion chamber or by allowing the α-particles to pass through a shallow ionization chamber which was then moved along until the

particle terminated its range in the chamber. The ranges displayed in range–energy curves are by convention mean ranges, i.e. the average range of a group of particles initially of homogeneous velocity. The range–energy relation for α-particles of energy up to 14 MeV is given in Fig. 3.14a. For other materials, these α-particle ranges are found empirically to vary as $A^{1/2}/\rho$, where A is the atomic weight and ρ the density of the absorber.

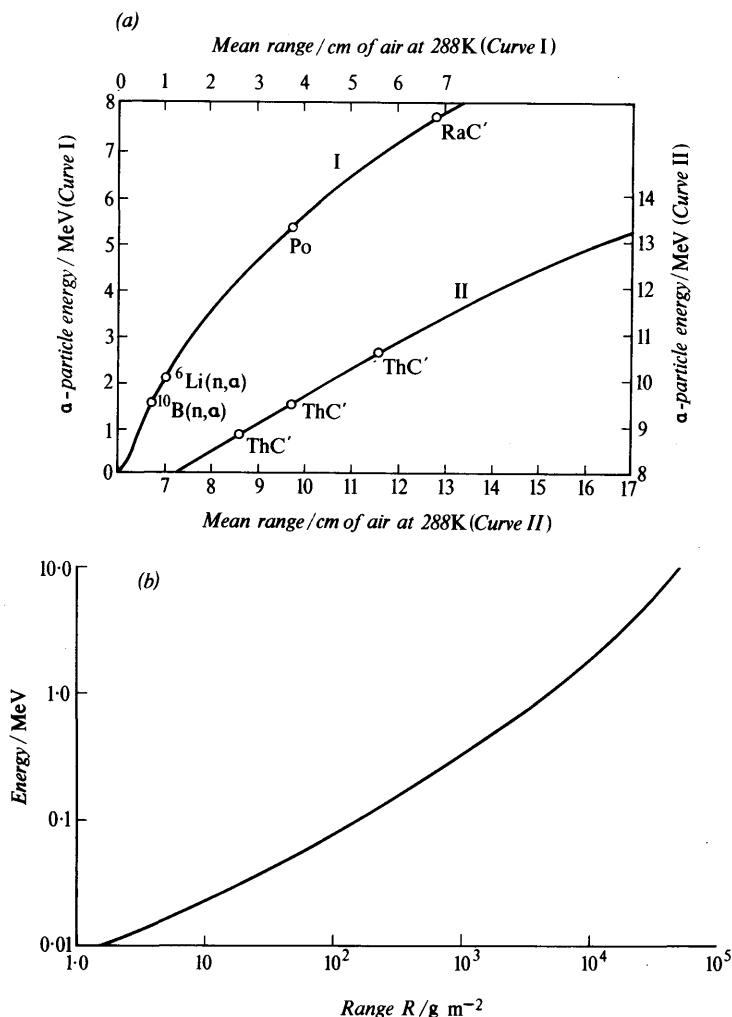Fig. 3.14   Range–energy curves: (*a*) α-particles 0–14 MeV, showing reactions or radioactive bodies used to provide calibration points (Ref. 2.1). (*b*) Electrons 0·01–10 MeV (Katz, L. and Penfold, A. S., *Rev. Mod. Phys.*, **24**, 28, 1952).

The range–energy curves for different particles may be connected by use of the stopping-power formula, equation (3.1). Since dT/dz' depends only on the charge (Z_1^2) and the particle velocity (v) for a given stopping material, it follows that the range for non-relativistic particles of given velocity is proportional to M/Z_1^2; e.g. protons, deuterons and tritons of energies 10, 20 and 30 MeV have ranges in the ratio 1:2:3.

The range of a slow electron in matter, as noted in Section 3.1.1, will be much less than its path length because of large-angle scattering. Ranges are therefore normally defined by the extrapolation procedure illustrated in Fig. 3.1*b*; this procedure is sufficiently reproducible to permit such ranges, both for homogeneous electrons and β-ray distributions, to be used in establishing a range–energy curve (Fig. 3.14*b*). To a good approximation, ranges expressed in $g\,m^{-2}$ (i.e. as mass per unit area, which is just proportional to the total number of electrons per unit area) are independent of the material of the absorber. The relation $R/g\,m^{-2}\,Al = 5430(E_0/MeV) - 1600$, first given by Feather, has been much used for finding the maximum energy in a β-ray spectrum.

An average α-particle from a radioactive source makes about 10^6 collisions resulting in small energy transfers before coming to rest in an absorber. A group of such particles initially of uniform velocity will show a distribution of velocities about a mean value after passage through a certain thickness of matter owing to the statistical nature of the energy loss. The ranges of the particles will, therefore, be grouped about a mean value, and since the number of collisions is large, the distribution of ranges may be well represented by a Gaussian curve. Figure 3.15*a* shows the results of an experiment to investigate the energy straggling of ^{241}Am α-particles; the standard deviation of the range distribution is about 1 per cent.

Most measurements of the energy of particles from nuclear reactions (say up to 50 MeV) are now based on complete absorption of the particle in a solid-state detector, rather than on measurements of range. In such detectors the number of electron–hole pairs, from which the output signal is derived, follows a Poisson distribution with standard deviation $\sigma = \sqrt{N}$ where N is the average number. In fact, as pointed out by Fano, the individual events are not independent because of the fixed total energy that may be lost and the resulting correlation narrows the distribution. For α-particles of energy 6 MeV a line width of 0·2 per cent is obtainable.

The slowing down of electrons in matter inevitably introduces a large straggling which is not only considerably greater in proportion than that for heavy particles but is also asymmetric, because of the high probability of loss of a large amount of energy in a single collision. The distribution of energy loss has been calculated by Landau and by others and is illustrated by the results of Goldwasser
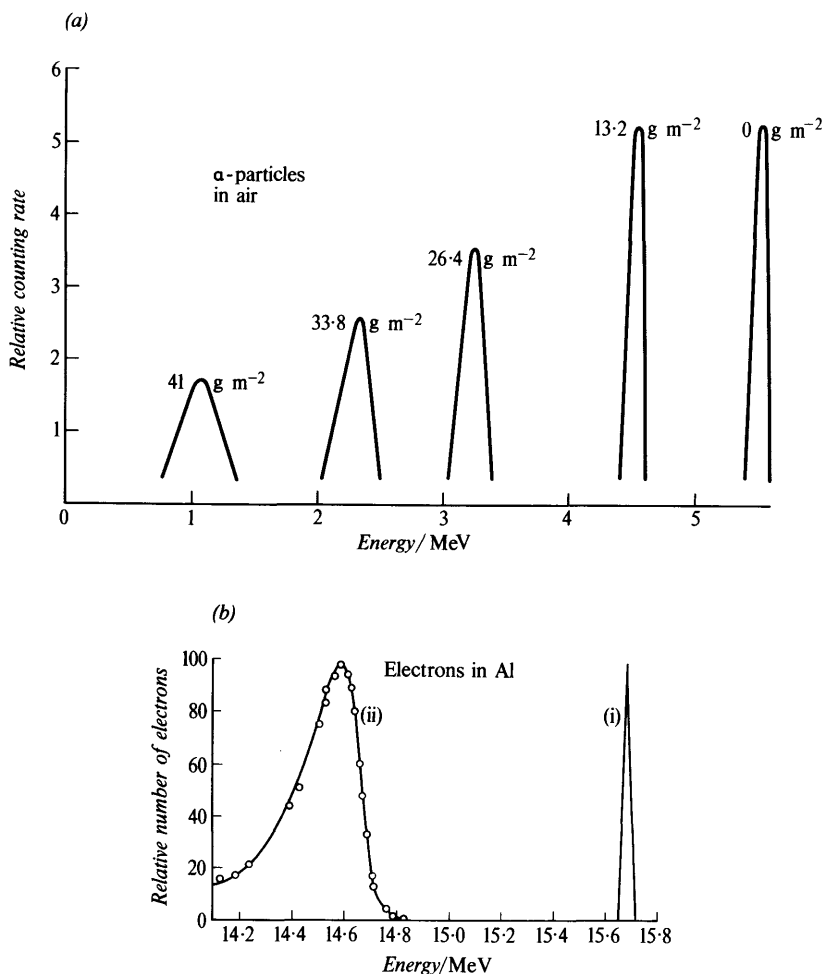
(a)

(b)

Fig. 3.15   (*a*) Energy distribution of 5·5-MeV α-particles from ^{241}Am after passing through indicated thicknesses of air. (*b*) Energy distribution of electron beam after passing through 8·6 kg m^{-2} of aluminium: (i) incident beam, (ii) transmitted beam (Goldwasser, E. L. *et al.*, *Phys. Rev.*, **88**, 1137, 1952).

et al. on the energy loss of 15·7-MeV electrons in a thin metal foil (Fig. 3.15*b*). The width of the Landau distribution has been measured and compared with theory for protons, electrons and muons and must always be taken into account in computing the most probable energy loss of a fast particle. As the velocity of the particle decreases, the relative importance of small energy transfers increases and the straggling tends to the symmetrical Gaussian form.

3.2.3 Capture and loss: stopping power for heavy ions

Near the end of the range of an α-particle in matter, the capture and loss of electrons by the ion, or charge exchange, i.e.

$$\left.\begin{array}{c} e^- + He^{++} \leftrightarrows He^+ \\ e^- + He^+ \rightleftarrows He^0 \end{array}\right\} \quad (3.23)$$

occurs very frequently. Experimentally observed cross-sections for helium ions of energy less than 1 MeV suggest mean free paths for processes (3.23) of a few thousandths of a millimetre for air at standard temperature and pressure. Charge equilibrium between the He^{++}, He^+ and He^0 components of a low-energy α-particle beam is thus reached for extremely thin layers of matter. Similar considerations apply to protons of low velocity, which may capture electrons to form neutral atoms.

Charge exchange is important for heavy ions, including fission fragments, and has been extensively studied because of the interest in establishing range–energy relations for such particles. These are required, for instance, in recoil methods of finding nuclear lifetimes (Sect. 9.4.1). For heavy ions, the velocity range over which electron exchange processes take place is much greater than for protons or α-particles and the energy loss per unit path is determined not by the atomic number Z_1 of the ion but by something approaching a root-mean-square (r.m.s.) value of the actual instantaneous charge as reduced by the number of retained electrons.

The r.m.s. charge of a heavy ion is highly velocity dependent and is governed by the principle that on average, and allowing for the essentially fluctuating nature of charge exchange processes, electrons whose orbital velocity in the ion is less than the ionic velocity will normally be lost. As an ion slows down from high velocities, at which the normal fully stripped rate of energy loss given by equation (3.1) is observed, more and more electrons are retained after capture from atoms of the stopping medium until finally a neutral atom state is reached. Ionization and excitation processes along the particle path diminish in accordance with the r.m.s. charge. This is clearly shown by the tapered appearance of heavy-ion tracks in nuclear emulsion, which is due to diminution in the number of δ-ray electrons produced by collision. Because of severe charge reduction the stopping power for heavy ions passes through a maximum as the ion velocity decreases, which accentuates the similar effect observed for protons and α-particles.

At very low velocities, it is predicted from calculations based on atomic models that the stopping power of matter for heavy ions should vary directly as the velocity $v = \beta c$. Especially at velocities for which this is true, but to some degree at all energies, there will be a loss of energy directly to the nuclei of the absorbing medium,

since such energy transfer varies as β^{-2}, from equation (3.1). Eventually, the nuclear stopping also passes through a maximum and decreases to zero as the heavy ion gradually becomes a neutral atom. The transfer of energy to neutral atoms leads to little additional ionization, and in contrast with transfer to electrons, is subject to very large statistical fluctuations, because the energy transfers are relatively larger and fewer in number. This seriously impairs the resolution of solid-state detectors (Sect. 4.5.2) for heavy ions.

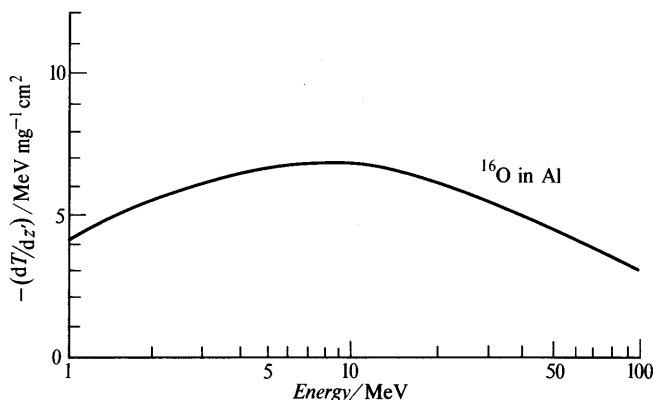Figure 3.16 shows the variation of stopping power with energy for ^{16}O ions in aluminium.

Fig. 3.16   Stipping power of aluminium for oxygen ions (Booth, W. I. and Grant, J. S., *Nuclear Physics*, **63,** 481, 1965).

3.2.4 Passage of charged particles through crystals; channelling

In Section 3.1.2 the theory of energy loss by collision was developed on the assumption of an isotropic medium in which the distribution of impact parameters b for collision with electrons could be written in the form $2\pi b\,db$. If a charged particle moves through a single crystal, however, the crystal structure defines certain directions or planes for which the electron density may be especially low, so that within a small range of angles ($\approx\frac{1}{10}°$ about these directions in typical cases) the impact parameter distribution may differ considerably from the isotropic form. In these directions, e.g. directions of high symmetry, there is increased penetration and finely collimated incident ions emerge from a thin crystal with an energy loss smaller than that which they experience in other directions. This phenomenon is known as *channelling;* for random angles of incidence and in amorphous solids the energy loss corresponds with the average electron density normally used in stopping-power calculations.
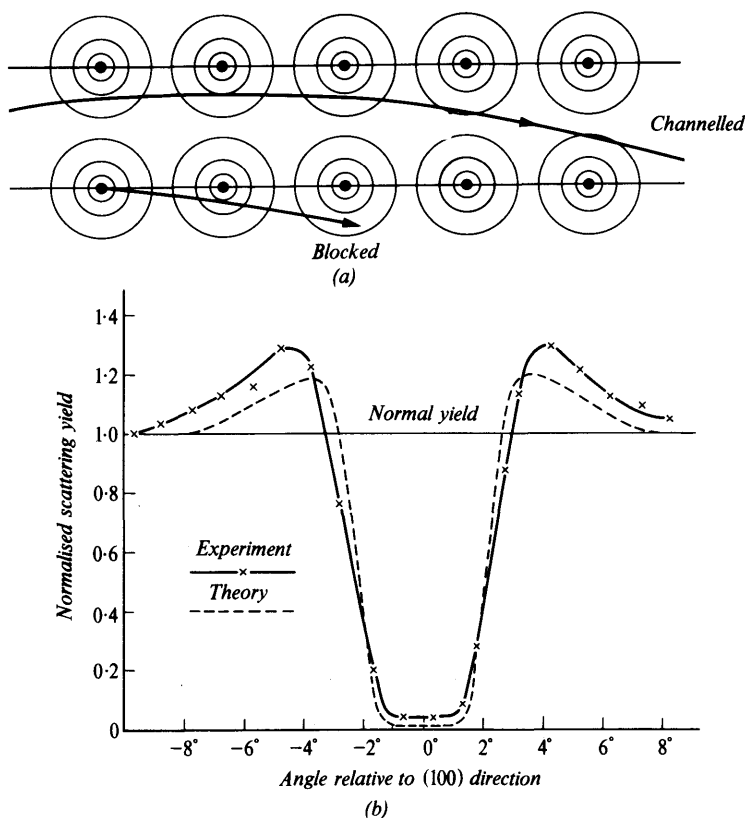
Fig. 3.17   Channelling and blocking: (*a*) Trajectories of ions between rows of atoms. A particle incident nearly parallel to the row is channelled; a particle emitted from a lattice site is scattered away from the channelling direction. The circles represent the atomic electron density. (*b*) Blocking dip in 135° Rutherford scattering of 480-keV protons incident, with an angular spread of 0·1°, along the ⟨100⟩ direction of a tungsten crystal (Andersen, J. U. and Uggerhoj, E., *Can. Jnl. Phys.*, **46**, 517, 1968).

The occurrence of channelling in a simple two-dimensional case is illustrated in Fig. 3.17*a*. An ion travelling in approximately the direction of a crystal axis approaches an atom and finds itself in a net repulsive field deriving from the resultant of the ion–nucleus and ion–electron interactions. This deflects the incident particle slightly towards the region of low electron density between the atomic rows. At the next atom of the row a similar effect occurs and as a result of the correlated series of Coulomb scatterings the ion moves from side to side between the rows of atoms. It is therefore steered through the crystal mainly in a region of low electron density and its energy loss per unit path is correspondingly reduced. It also tends to avoid

94

close nuclear collisions. Such effects will be enhanced for heavy ions, for which it has already been noted that nuclear stopping may be important in comparison with electronic loss. Channelling is also observed, however, for light particles of an energy of several MeV, for electrons and for mesons.

An effect closely allied to channelling is the *blocking* of the emission of charged particles from lattice sites. Because of the strong Coulomb deflections, particles will not be able to enter a direction of crystal symmetry over a small range of angles. Nuclear reactions and large-angle Coulomb scattering provide convenient sources of particles leaving lattice points and yields show a marked dip as a crystal target is rotated round a beam direction because close collisions are inhibited over a small angular range. Figure 3.17*b* shows results obtained for back-scattered protons.

3.2.5 *Examples of the use of the stopping-power formula*

In the series of experiments leading to our first knowledge of the mass of the pion m_π use was made of the following quantities related to energy loss, mainly in nuclear emulsion, and for non-relativistic particles:

(*a*) range R;
(*b*) grain density g;
(*c*) mean multiple-scattering angle.

In addition, particle momenta p were known from magnetic deflection experiments. It was assumed from the visual evidence of pion decay to a muon and then to an electron that the pionic charge was equal to that of the electron.

To obtain a mass value, two observed quantities must be used, since each quantity is velocity dependent. From the stopping-power formula (eqn (3.1) and Sect. 3.2.2), the range of a pion of velocity β is

$$R_\pi = m_\pi / Z_\pi^2 \cdot f_1(\beta) \qquad (3.24)$$

and the corresponding grain density, proportional to energy loss, is

$$g_\pi = Z_\pi^2 f_2(\beta) \qquad (3.25)$$

Similar equations can be written for protons, and if the pion is compared with a proton of the same β, as defined by grain density, then $R_\pi / R_p = m_\pi / m_p$.

Alternatively, the mean multiple-scattering angle per unit path length, which is proportional to $(p\beta)^{-1}$ by equation (3.21), may be found for a pion of known range. If a range–energy relation for protons in emulsion is known then that for pions may be deduced in
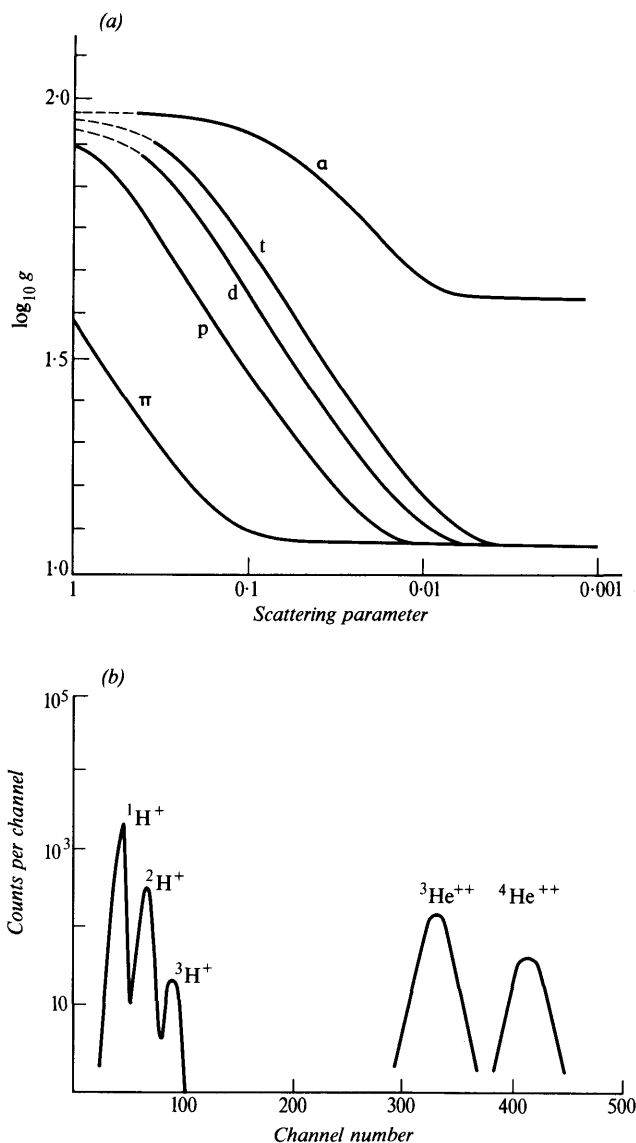
Fig. 3.18   Identification of charged particles: (*a*) Relation between number of grains *g* per 50 μm of a particle track in nuclear emulsion and the average angular displacement per 100 μm of track (Powell, C. F., *Reports on Progress in Physics*, **13**, 350, 1950). (*b*) Mass spectrum of particles from the reaction ^{27}Al + ^{3}He at 30 MeV using the $T - \Delta T$ identification system (England, J. B. A., *Nucl. Instrum. Meth.*, **106**, 45, 1973).

terms of m_π. The observations of $p\beta$ and R_π then permit elimina-
tion of the velocity β and deduction of the mass. Instead of range
measurements, it is also possible to use grain density observations
since this quantity is also velocity dependent. Figure 3.18*a* illus-
trates the discrimination between particles obtained in this way.

Similar use may be made of direct measurements of the momen-
tum p and residual range R_π, but this, like the former method, is
dependent on knowledge of the proton range–energy relationship.
This may be avoided if magnetic deflection experiments are used to
compare the momenta p_π and p_p of pions and protons of known
range. If the initial velocities β_π and β_p are the same we have from
equation (3.24)

$$R_\pi/R_p = m_\pi/m_p = p_\pi/p_p \qquad (3.26)$$

so that the mass ratio is known when the ratio of ranges is equal to
the ratio of momenta. Such an experiment was conducted with a
cyclotron producing both protons and pions with a range of ener-
gies, and momenta were obtained by noting the deflection of these
particles in the magnetic field of the cyclotron itself.

A more modern technique widely used in particle detection
systems for mass discrimination is to combine an energy-loss signal
from a thin 'passing' counter with a total energy signal from a thick
counter in which the particles stop. The product $T\, dT/dz'$ is propor-
tional, for non-relativistic particles, to $(\tfrac{1}{2}M_1 v^2)Z_1^2/v^2$, i.e. to $M_1 Z_1^2$,
independently of energy; Fig. 3.18*b* gives a mass spectrum obtained
in this way in a nuclear reaction experiment.

3.3 Exotic atoms

The final state of an ion slowed down in matter is an atom formed
by complete neutralization of the ionic charge by electron capture.
The behaviour of elementary particles coming to rest in matter
reflects their intrinsic nature. Thus positrons, which are stable,
disappear by annihilation with electrons, but before they do so, may
form a hydrogen-like atom of positronium (e^+e^-) some of whose
properties can be studied during times of the order of the triplet
^{3}S-state lifetime of $\approx 10^{-7}$ s. Antiprotons are hadronic and only
reach low velocities if they escape nuclear interactions in matter. In
hydrogen they may form *protonium* $(p\bar p)$ as a preliminary to annihi-
lation, mainly into pions.

Muons and charged pions, kaons and hyperons have lifetimes
between 10^{-6} and 10^{-10} s and some therefore survive a slowing-
down process which takes 10^{-10} to 10^{-9} s. The positively charged
particles are kept away from the nuclei of the stopping material by
Coulomb repulsion and disappear by normal decay processes. The
negative particles, however, may enter a hydrogen-like bound
atomic state in the Coulomb field of a nucleus, forming an *exotic*

atom. The particle may exist in this atomic state until decay takes place or it may promote a nuclear interaction. The structures discussed here are, of course, essentially different from hypernuclei (Sect. 2.4) in which the nucleus itself is unusual.

In exotic atom formation the slowed-down particle is normally captured into a state of high principal quantum number and reaches lower states in perhaps 10^{-13}–10^{-14} s by a series of transitions in which radiation (or Auger electrons) is emitted. The Bohr radius $a_0 = 4\pi\varepsilon_0^2\hbar^2/m_x e^2$ for an exotic atom is smaller by a factor m_x/m_e than that for electronic hydrogen and this factor is at least 207, its value for the muon. Similarly, the transition energies for the exotic atom are *greater* by the same factor and may be in the X-ray (keV) or nuclear (MeV) range of energies. The importance of exotic atoms lies in the fact that the wavefunction of the bound particle in all states, and especially in the lowest s-state if this is reached, overlaps the nucleus much more strongly than do the normal electronic wavefunctions. The finite size of the nucleus results in a diminution in transition energies compared with what would be expected for a point charge, and the diminution for the lower states is a major effect that is easily observed, in contrast with the same effect for electrons.

Muons interact only weakly with nuclei and normally reach the ground state of the muonic atoms that they form. The highest energy radiations observed are the muonic K X-rays due to the transition $2p \rightarrow 1s$; for the element titanium, for instance, these have an energy of 1 MeV. Extensive and accurate measurements of μK X-ray energies have contributed much information on the radius of the nuclear charge distribution. Precision measurements of transitions between the outer muonic levels, e.g. $3d \rightarrow 2p$ for which the nuclear size effect is smaller, give an accurate value for the muon mass.

Pionic atoms have been used in the same way to determine the mass of the pion, e.g. from the energy of the transition $4f \rightarrow 3d$, which has a value of $87\cdot622 \pm 0\cdot001$ keV in pionic titanium. The pion interacts strongly with nuclei and for atoms with Z greater than about 12, nuclear absorption from the 2p state takes place with greater probability than radiation, so that the πK X-rays are not observed. For a similar reason, pionic atoms are less useful than muonic atoms for nuclear size determinations.

In kaonic atoms, nuclear absorption is an even stronger effect and takes place from states with high quantum numbers. The cut-off of kaonic X-rays of a particular atomic sequence, e.g. $5g \rightarrow 4f$, as Z increases, shows the onset of absorption from a particular state, e.g. 5g, and provides a sensitive probe of the nuclear density distribution at large radii. Identification of the reaction products shows whether the kaon has interacted with a neutron or a proton.

3.4 Hyperfine effects in atoms

The interaction of nuclei with the extra-nuclear structure of elec-
trons (and other particles in the case of exotic atoms) that surrounds
them is an important source of information on nuclear angular
momentum, nuclear moments and nuclear size. The effects of these
nuclear properties are manifest in optical, microwave and radio-
frequency spectroscopy. Because of the small scale of the energy
splittings compared with the fine structure of optical lines, they are
generally described as *hyperfine* effects. They are additional, of
course, to the effect of the basic Coulomb attraction that binds the
atom and defines the gross structure of the atomic energy spectrum,
and to the fine structure of these levels arising from the electronic
spin–orbit interaction.

3.4.1 Definitions

The following quantities, some of which have been introduced in
Section 1.2.6, are required in a discussion of hyperfine effects:

(a) *The nuclear angular momentum vector* I, with absolute mag-
    nitude

$$|I| = \sqrt{I(I+1)}\ \hbar \qquad (3.27)$$

where I, the nuclear spin quantum number, is integral or half-
integral. In accordance with the uncertainty principle, the direc-
tion in space of the vector I cannot be determined, but if an axis
Oz of quantization is defined, e.g. by an external magnetic field,
the component of I along Oz will be observable and will have
the value $m_I \hbar$ where m_I has one of the $2I+1$ values I,
$(I-1), \ldots, -(I-1), -I$. In a vector diagram I is considered to
lie on a cone described round the axis Oz with semi-angle β
given by

$$\cos \beta = m_I \hbar / |I| = m_I / \sqrt{I(I+1)} \qquad (3.28)$$

The maximum value of the component of I is $I\hbar$ and this is
usually known as the nuclear spin.

(b) *The nuclear magnetic moment vector* μ_I, which is a vector
    parallel or anti-parallel to I. It may be expressed in absolute
    units or in nuclear magnetons, defined as $\mu_N = eh/4\pi m_p$ in
    analogy with the Bohr magneton, but smaller by a factor of
    $m_e/m_p = \frac{1}{1836}$. The observable nuclear magnetic moment μ_I is the
    expectation value of the z-component of the vector operator μ
    in the state $(I, m_I = I)$ in which m_I has its maximum value.

(c) *The nuclear gyromagnetic ratio* γ_I, equal to the nuclear moment in absolute units divided by the nuclear spin also expressed in these units, i.e.

$$\gamma_I = \boldsymbol{\mu}_I/\boldsymbol{I} = (\boldsymbol{\mu}_I/\boldsymbol{I})_z \quad \text{or simply} \quad \mu_I/I\hbar \qquad (3.29)$$

The ratio of the nuclear moment expressed in nuclear magnetons to the nuclear spin expressed in units of $\hbar$ is defined to be the dimensionless nuclear *g-factor* g_I and is related to γ_I by the equation

$$g_I = \gamma_I 2m_p/e \qquad (3.30)$$

If the nuclear moment and spin are oppositely directed, as in the case of the neutron, μ_I, γ_I and g_I are negative. The g-factor defined in (3.30) has a value of the order of unity. For some purposes it has become customary to use nuclear g-factors defined in terms of the Bohr magneton and these g-factors are then of the order of $\frac{1}{2000}$. From (3.29)

$$\mu_I = \gamma_I I\hbar = g_I I\mu_N \quad \text{or} \quad g_I I\mu_B \qquad (3.31)$$

(d) *The nuclear electric quadrupole moment,* Q_0, which measures the deviation of the nuclear charge distribution from a spherical shape. If the nucleus has symmetry about an axis Oz' fixed in itself (Fig. 3.19) and if the charge density is ρ then the *intrinsic* quadrupole moment Q_0 is defined by the equation

$$eQ_0 = \int \rho(3z'^2 - r'^2)\,d^3r' = \int \rho r'^2 (3\cos^2\theta' - 1)\,d^3r' \qquad (3.32)$$

where d^3r' is the volume element and $\int \rho\, d^3r'$ for the whole nucleus is equal to Ze.

This is a purely classical definition and the quantity multiplying the element of charge is directly derivable from an expansion of the electrostatic potential at a distant point due to a charge distribution. This expansion also contains an electric dipole term, but if the nucleus (or atom) is in a state of well-defined parity the electric dipole moment vanishes. This is because in the quantum mechanical expression for the dipole moment the charge density ρ is replaced by the even function $e\,|\psi|^2$ and this is multiplied, not by a quantity containing squared terms such as $\cos^2\theta'$ as in (3.32), but by $\cos\theta'$. Integration over the nuclear volume then gives zero.

The observable electric quadrupole moment Q_I is the expectation value of a quadrupole operator (similar to 3.32) in the state I, $m_I = I$ in which m_I has its maximum value. It is less than the intrinsic moment Q_0 because the axis of nuclear spin cannot be completely aligned with the space-fixed axis Oz. In terms of the angle β given in equation (3.28) with $m_I = I$, it may be
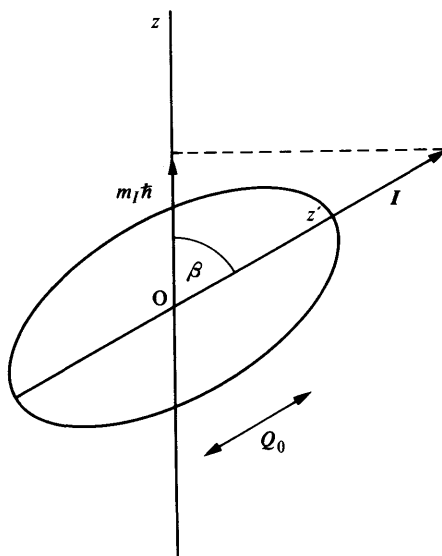
Fig. 3.19   Nuclear quadrupole moment. In this diagram both the intrinsic angular momentum I and the intrinsic quadrupole moment Q_0 are related to the body-fixed axis Oz'. Observable values I ($= m_I^* \hbar$) and Q_I are defined with respect to the space-fixed axis Oz.

shown that

$$Q_I = \tfrac{1}{2}(3\cos^2\beta - 1)Q_0 = (2I - 1)/2(I + 1)Q_0 \qquad (3.33)$$

Arguments similar to that given for the electric dipole moment above show that Q_I exists only for states with $I \geqslant 1$, even when Q_0 is finite.

The sign of Q_I is that of Q_0, i.e. negative for an oblate and positive for a prolate (cigar-shaped) nucleus. It is measured in m^2 or *barns* ($10^{-28}\,m^2$). Usually, tables give the values of Q_I rather than Q_0.

3.4.2 The magnetic interaction

In the absence of external fields, magnetic interaction arises from the fact that the nuclear magnetic moment finds itself in a field of magnetic induction B_i arising from the electronic motion in the rest of the atom (or crystal), with associated angular momentum J. The intrinsic magnetic moment of the electron contributes to B_i and, in fact, wholly determines it in the case of a hydrogen-like atom with a single s-electron. We shall consider only atoms with a single valence electron.

The total mechanical angular momentum of the atom is F, where

$$F = I + J \tag{3.34}$$

This vector sum can be performed in either $2I + 1$ or $2J + 1$ different ways according to the relative magnitudes of I and J, and each arrangement corresponds to a different relative orientation of the vectors I, J. In such a vector model, as in the case of the coupling of L and S vectors in the atom, the individual vectors I, J are taken to precess round the direction of their resultant F and this may be understood as a result of the couple $\mu_I \times B_i$ arising between the magnetic moment μ_I, parallel to I and the internal field B_i, assumed parallel to J.

In a state of total angular momentum F the interaction energy, which is a component of the total energy of the atom, is

$$W_F = -\mu_I \cdot B_i = -a I \cdot J \tag{3.35}$$

where a is a magnetic interaction constant. The value of the scalar product $I \cdot J$ can be evaluated for an eigenstate of the system by noting that

$$F^2 = I^2 + J^2 + 2 I \cdot J$$

and inserting the eigenvalues of the squared vector operators

$$I \cdot J = \tfrac{1}{2}[F(F+1) - I(I+1) - J(J+1)]\hbar^2$$
$$= \tfrac{1}{2}C, \quad \text{say}, \tag{3.36}$$

so that

$$W_F = -aC/2 \tag{3.37}$$

and the energy levels of the atom are split into a group of states whose number may be determined by the nuclear spin (when $|I| < |J|$) and whose separation is dependent on the nuclear moment (through a). This group of states is known as the *hyperfine structure* and is shown for the $^2S_{1/2}$ ground state of hydrogen and for the $^2S_{1/2}$ ground state and $^2P_{1/2}$ excited state of sodium in Fig. 3.20a. The order of the levels follows from the fact that because of the negative electronic charge B_i is generally of opposite sign to J; the nuclear moment is positive in both cases, so that a in (3.35) and (3.37) is negative.

The *hyperfine splitting* ΔW between the states F and $F - 1$ is equal to aF from (3.37). The interaction constant a can be calculated for a simple atomic structure; for the ground state of hydrogen it corresponds to a frequency difference

$$\Delta \nu = h^{-1} \Delta W = 1420 \text{ MHz}$$

and this transition gives rise to the celebrated 21-cm line of astrophysics, which is an indicator of the presence of atomic hydrogen.

For the ground state of sodium the corresponding frequency is about 1800 MHz; the hyperfine structure of the ground and first excited state is elegantly shown (Fig. 3.20b) by observing the intensity of tunable dye-laser light scattered from a sodium atomic beam as the laser frequency is varied near the frequency of one of the D-lines.
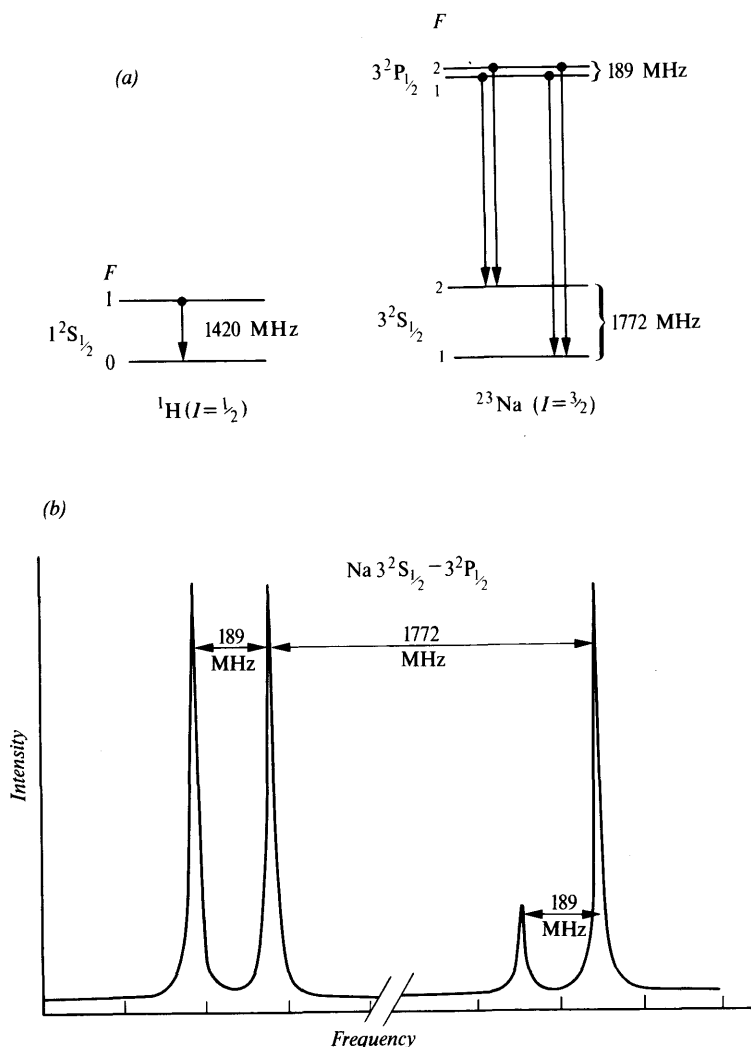

Fig. 3.20   (a) Hyperfine structure of ground state of hydrogen and of $3^2S_{1/2}$, $3^2P_{1/2}$ states of sodium. (b) Study of sodium hyperfine structure by scattering of laser light from a sodium atomic beam.

Magnetic hyperfine effects are observable in the spectra of muonic atoms and also, on a magnified scale, in positronium for which the 'nucleus' has a moment of μ_B.

3.4.3 The electrostatic interaction

Hyperfine effects arising from the interaction of the nuclear electric quadrupole moment with an electrostatic field *gradient* at the nucleus due to the electronic structure were first observed as deviations of hyperfine structure separations from the prediction $\Delta \nu = aF/h$ based on an exclusively magnetic interaction.

The theory of the electrostatic interaction is more complicated than that for the magnetic interaction (Sect. 3.4.2) and will not be given here. Deduction of the moment Q_I from the observed quadrupole displacements in atomic spectra requires knowledge of the internal electric field gradient, which must be predicted from an atomic model.

Electrostatic hyperfine effects in ordinary atoms tend to be smaller than the magnetic hyperfine structure, but in muonic atoms the muonic magnetic moment is scaled down by m_e/m_μ with respect to the Bohr magneton and the quadrupole effect is more important.

3.5 Summary

This chapter surveys the interactions between particles and radiation and their environment, as far as phenomena of relevance to nuclear physics are concerned. Charged particles lose energy by collisions with electrons; in addition, fast electrons may radiate bremsstrahlung. Electromagnetic radiation itself for energies of the order of 1 MeV and above undergoes the characteristic photoelectric, Compton and pair production interactions. In experimental measurements, account must be taken of the fluctuation phenomena leading to multiple scattering, straggling and charge exchange.

The electromagnetic interaction dominates energy-loss processes. Since it also binds ordinary electrons to nuclei in atoms, the corresponding bound states of some fundamental particles are examined. In all atoms hyperfine effects due to nuclear moments are also mediated by the electromagnetic field.

Examples 3

3.1* Verify the statement (eqn (3.2)) that under a certain condition the maximum transfer of energy from a charged particle of velocity v to an electron is $2m_e v^2/(1 - \beta^2)$ (use the four-vector expression for energy-momentum).

3.2 Assuming that equation (3.1) were rigorously true at low energies, show that the stopping power reaches a maximum value as the velocity decreases. Find

the energy of protons in aluminium for which this maximum would be expected, assuming that $I = 150$ eV. [187 keV]

3.3 From the simple theory outlined in Section 3.1.2 show that the cross-section for transferring an energy between Q and $Q + dQ$ to a free electron in the collision is given by

$$d\sigma = (Z_1^2 e^4 / 8\pi\varepsilon_0^2 m_e v^2) \, dQ/Q^2$$

3.4 An α-particle is found to have a range of 300 μm in a nuclear emulsion. What range would you expect for (a) a ^{3}He nucleus, (b) a ^{3}H nucleus, each of the same initial velocity as the α-particle? [225 μm, 900 μm]

3.5 Figure 3.1a suggests that a beam of α-particles suffers no loss·by scattering at least until the particles are near the end of their range. Using an averaged scattering cross-section of 3×10^{-26} m^2, investigate this assumption for a beam of 5-MeV α-particles in nitrogen.

3.6 A thin ionization chamber is traversed successively by a 10-MeV proton, a 20-MeV deuteron, a 30-MeV ^{3}He particle and a 40-MeV α-particle. Calculate the relative size of the ionization pulses produced (omit the logarithmic term in eqn (3.1)). [1, 1, 4, 4]

3.7 At ·what energies have the following particles a collision loss in Al of 175 keV mg^{-1} cm^2: electron, muon, proton, deuteron, α-particle? (Use Fig. 3.4 and eqn (3.1) and omit the variation due to the logarithmic term.) [0·5 keV, 0·11, 1, 2, 16 MeV]

3.8 A kaon of kinetic energy 0·1 GeV slows down in an aluminium absorber. Using the collision-loss formula, and assuming an average value of 5 for the logarithmic term, find how long it takes to reach an energy of 1000 eV. Make any reasonable assumptions necessary. [$\approx 10^{-10}$ s]

3.9* Calculate the momentum transfer required in the absorption of a pion by a nucleon in a complex nucleus. What conclusion may be drawn from the magnitude of this transfer, if the Fermi momentum in the nucleus is given by $k_F = 1·36$ fm^{-1}?

3.10 In an experiment with a source of X-radiation the mass attenuation coefficients μ/ρ for the elements Al, Ti, Cu are found to be 9·97, 37·7 and 9·97 m^2 kg^{-1} respectively (the atomic numbers are 13, 22 and 29). Explain qualitatively the result for Ti.

3.11 A beam of X-radiation is attenuated by a factor of 0·64 in passing through a block of graphite of thickness 0·01 m. Assuming that the attenuation is due only to classical Thomson scattering, with a total cross-section of $6·7 \times 10^{-29}$ m^2 per electron, estimate the atomic number of carbon.

3.12 Calculate for the Compton scattering of X-rays of wavelength 0·01 nm: (a) the wavelength of the scattered radiation at 45°; (b) the velocity of the corresponding recoil electron; (c) the momentum transfer to the electron. [0·0107 nm, $5·3 \times 10^7$ m s^{-1}, 93 keV/c]

3.13 Calculate the energy of a 100-keV photon scattered backwards ($\theta = 180°$) from an electron of energy 1000 keV moving towards the photon. [1015 keV]

3.14 What is the energy of Compton-scattered photons at 90° when $h\nu \gg m_e c^2$? [511 keV]

3.15* Show that the threshold quantum energy for the production of an electron–positron pair in the field of a free electron is $4m_e c^2$.

3.16 A triton (^{3}H) of energy 5000 MeV passes through a transparent medium of refractive index $n = 1·5$. Calculate the angle of emission of Cherenkov light. [44°]

3.17 Calculate the number of photons produced per metre of air ($n = 1·000\,293$) by the Cherenkov effect from the path of a relativistic electron in the wavelength range $\lambda = 350$ to 550 nm. [27]

3.18 Show that in the annihilation of positrons at rest by electrons of momentum p, the angle between the two annihilation quanta is $\pi - p_\perp/m_e c$ where $p_\perp$ is the momentum of the electron at right angles to the line of flight of the quanta.

3.19* For the two-quantum annihilation of a fast positron of kinetic energy T by a free electron at rest, show that the energy of the forward going annihilation radiation is approximately $T + \frac{3}{2}m_e c^2$.

3.20* Calculate the angle between coupled I and J vectors for the case $I = \frac{3}{2}$, $J = \frac{1}{2}$, $F = 2$ or 1 (e.g. ^{23}Na).